Optical control of molecular dynamics: Molecular cannons, reflectrons, and wave-packet focusers

Jeffrey L. Krause, Robert M. Whitnell, Kent R. Wilson, and YiJing Yan
Department of Chemistry, University of California, San Diego, La Jolla, California 92093-0339

Shaul Mukamel
Department of Chemistry, University of Rochester, Rochester, New York 14627

(Received 15 April 1993; accepted 21 July 1993)

We consider the control of molecular dynamics using tailored light fields, based on a phase space theory of control [Y. J. Yan *et al.*, J. Phys. Chem. **97**, 2320 (1993)]. This theory enables us to calculate, in the weak field (one-photon) limit, the globally optimal light field that produces the best overlap for a given phase space target. We present as an illustrative example the use of quantum control to overcome the natural tendency of quantum wave packets to delocalize on excited state potential energy curves. Three cases are studied: (i) a "molecular cannon" in which we focus an outgoing continuum wave packet of I_2 in both position and momentum, (ii) a "reflectron" in which we focus an incoming bound wave packet of I_2, and (iii) the focusing of a bound wave packet of Na_2 at a turning point on the excited state potential using multiple light pulses to create a localized wave packet with zero momentum. For each case, we compute the globally optimal light field and also how well the wave packet produced by this light field achieves the desired target. These globally optimal fields are quite simple and robust. While our theory provides the globally optimal light field in the linear, weak field regime, experiment can in reality only provide a restricted universe of possible light fields. We therefore also consider the control of molecular quantum dynamics using light fields restricted to a parametrized functional form which spans a set of fields that can be experimentally realized. We fit the globally optimal electric field with a functional form consisting of a superposition of subpulses with variable parameters of amplitude, center time, center frequency, temporal width, relative phase, and linear and quadratic chirp. The best fit light fields produce excellent quantum control and are within the range of experimental possibility. We discuss relevant experiments such as ultrafast spectroscopy and ultrafast electron and x-ray diffraction which can in principle detect these focused wave packets.

I. INTRODUCTION

Theoretical studies indicate that molecular dynamics (of chemical reactions, for example) can be guided and controlled by light fields whose temporal and frequency properties are properly tailored.[1–4] For detailed discussion, see the reviews by Brumer and Shapiro,[5] Rabitz,[6] Rice,[7] and Warren, Rabitz, and Dahleh.[8]

Most of the theoretical methods which have been developed to control molecular dynamics are based on a wave-function formalism which involves calculating the coupled quantum dynamics of the relevant degrees of freedom of the problem. Additionally, it is usually assumed that the system is initially in a pure state. Recently, we have cast the theory of optimal control of molecular dynamics in a phase space formalism based on the evolution of the density matrix.[9] This formulation allows the inclusion of mixed states (thermal ensembles or molecules in solution, for example) and provides a unified theory for quantum, classical, or semiclassical implementations of molecular dynamics.

In our previous work,[9] we showed that in the weak field or linear control regime, the globally optimal fields, as well as a variety of locally optimal control fields, for a given phase space target can be calculated from the solution of an eigenequation. As we shall review in more detail in Sec. II, the kernel of the eigenequation depends only on properties of the molecule and target, so it can be computed without reference to the field. The largest eigenvalue of this equation is, in the weak field limit, the globally optimal yield, and the eigenfunction corresponding to that eigenvalue is the globally optimal field.[9]

We have previously demonstrated the utility of this approach through application to excited state control of a model system consisting of shifted harmonic oscillators. We illustrated for this case that broadening the scope (and realism) of the material system to include the effects of temperature and of solvent does not necessarily eliminate the possibility of control. A substantial amount of control is still retained at room or higher temperatures, even when vibrational and/or electronic relaxation or dephasing is introduced through the presence of a model Brownian oscillator solvent.[9,10]

The proper theoretical representation of experimentally realizable molecular control requires consideration of both realistic molecular systems and experimentally realizable light fields. In the present work, we extend the applications of the density matrix formulation of optimal control. We first consider realistic molecular potentials, taking as illustrations the focusing of outgoing continuum I_2 wave packets (a "molecular cannon"), the focusing of bound

 0021-9606/93/99(9)/6562/17/$6.00

state I_2 wave packets with nonzero incoming momentum (a "molecular reflectron"), and the focusing of Na_2 wave packets at the turning point of the potential using multiple phase-locked light pulses.

The optimal weak fields predicted by our formalism are unrestricted with respect to their functional form. In general, however, experimentally realizable light fields are drawn from a much smaller universe. We therefore show in this work that fits of the globally optimal fields by experimentally reasonable functional forms produce fields that are able to control the molecular dynamics almost as well as their forebears.

The structure of the paper is as follows. Section II reviews the density matrix formalism of optimal control in the weak field limit and its application to the phase and configuration space control of molecular systems involving two electronic surfaces. In Sec. III, the globally optimal weak field control problem is illustrated for the three realistic molecular cases described above. In Sec. IV, control by a parametrized field is considered. The unrestricted fields from Sec. III are fitted to an experimentally reasonable functional form, and the degree of control achieved with these fitted parametrized fields is compared to the globally optimal unrestricted results. In addition, we discuss how to optimize the yield within a restricted universe of parametrized fields. Finally, Sec. V presents a summary of the key points of the paper, discusses possible experiments to observe wave-packet focusing using both ultrafast spectroscopy and ultrafast electron and x-ray diffraction, and concludes.

II. WEAK FIELD CONTROL OF MOLECULAR DYNAMICS

A. General theory

As in our previous work,[9] we consider a molecule with a time-independent Hamiltonian H_M which interacts with a time-dependent electric field $\epsilon(t)$. The Hamiltonian for the entire system is then given by

$$H(t)=H_M-D\epsilon(t), \tag{1}$$

where D is the transition dipole moment of the material. As before, we express the control theory in a density matrix formulation.[9] This formulation allows a convenient representation of mixed states[11] such as those which occur at nonzero temperatures or in solutions. The evolution of the density matrix of the system, $\rho(t)$, is governed by the Liouville equation[11]

$$\rho(t)=\mathcal{G}(t,t_0)\rho(t_0), \tag{2}$$

where $\mathcal{G}$ is the Green function associated with $H(t)$ [Eq. (1)], and t_0 is a time before the interaction with the light field.

We formulate the control problem in terms of a target operator $\hat{A}$. Chosen appropriately, this target operator, defined in phase space, can describe any desired outcome for a system.[6,9,12–14] The objective is to find the optimal light field such that the density matrix of the system, after interaction with this light field, has maximal overlap with the target operator at a specified time, t_f. In more formal terms, we define the yield of the control process as[9]

$$A(t_f)=\mathrm{Tr}[\hat{A}\rho(t_f)]. \tag{3}$$

Our goal, then, is to maximize $A(t_f)$.

In this paper, we work in the limit of weak light fields, in which the control outcome $[A(t_f)]$ is proportional to the external field intensity. That is, we consider only single-photon control processes in the limit that first-order perturbation theory is valid. In the wave-function formalism, the interaction of the wave function with the field is linear, and we apply first-order perturbation theory, while in the density matrix formalism, the interaction is bilinear. The weak field limit, depending on the system being studied, can be valid with quite intense electric fields. In fact, most spectroscopic measurements are performed in this limit.

We have shown that calculating the optimal electric field which maximizes $A(t_f)$ is straightforward. Through a perturbation theory treatment, the density matrix to second order in the control field is given by[11]

$$\rho^{(2)}(t_f)=(i/\hbar)^2\int_{t_0}^{t_f}d\tau_2\int_{t_0}^{\tau_2}d\tau_1\,\mathcal{G}_0(t_f-\tau_2)\times\mathcal{D}\mathcal{G}_0(\tau_2-\tau_1)\mathcal{D}\mathcal{G}_0(\tau_1-t_0)\times\rho(t_0)\epsilon(\tau_2)\epsilon(\tau_1). \tag{4}$$

Here, $\mathcal{G}_0$ is the Green function corresponding to the time-independent material Hamiltonian H_M rather than the full (time-dependent) Hamiltonian H and therefore depends only on a time difference rather than two independent values of time, as does the Green function in Eq. (2), i.e.,[11]

$$\mathcal{G}_0(t)\hat{O}=e^{-iH_Mt/\hbar}\hat{O}e^{iH_Mt/\hbar}, \tag{5}$$

where $\hat{O}$ is an arbitrary operator. In Eq. (4), $\mathcal{D}$ refers to the material dipole commutator,[11] $\mathcal{D}\hat{O}=D\hat{O}-\hat{O}D$. The initial time t_0 is taken to be $-\infty$ under the assumption that the system is initially in a steady state (e.g., thermal equilibrium or a molecular eigenstate) such that the initial density matrix $\rho(t_0=-\infty)$ commutes with the molecular Hamiltonian H_M at t_0, $[H_M,\rho(t_0)]=0$. In this case, $\mathcal{G}_0(\tau_1-t_0)\rho(t_0)=\rho(t_0)$.

In the weak field limit, the yield [Eqs. (3) and (4)] can be expressed as

$$A(t_f)=\hbar^{-2}\int_{t_0}^{t_f}d\tau_2\int_{t_0}^{\tau_2}d\tau_1\,M(t_f-\tau_2,\tau_2-\tau_1)\times\epsilon(\tau_2)\epsilon(\tau_1). \tag{6}$$

Here, the function M depends only on the material and the target and is given by

$$M(t_2,t_1)=-\mathrm{Tr}[\hat{A}\mathcal{G}_0(t_2)\mathcal{D}\mathcal{G}_0(t_1)\mathcal{D}\rho(-\infty)]. \tag{7}$$

Expanding Eq. (7) gives an expression that can be recast as

$$M(t_2,t_1)=2\,\mathrm{Re}[\langle D(0)\hat{A}(t_1+t_2)D(t_1)\rangle-\langle\hat{A}(t_1+t_2)D(t_1)D(0)\rangle] \tag{8}$$

with

$$\hat{A}(\tau)=\hat{A}\mathcal{G}_0(\tau)=e^{iH_M\tau/\hbar}\hat{A}e^{-iH_M\tau/\hbar} \tag{9}$$

and

$$D(\tau)=D\mathcal{G}_0(\tau)=e^{iH_M\tau/\hbar}De^{-iH_M\tau/\hbar}. \tag{10}$$

In Eq. 8, $\langle\hat{O}\rangle\equiv\mathrm{Tr}[\hat{O}\rho(t_0)]$ denotes an average over the initial material ensemble, $\rho(t_0=-\infty)$.

We wish to find the optimal field, $\epsilon(\tau)$, that maximizes the yield $A(t_f)$ [Eq. (3)] under the constraint that the energy of the field, $\int d\tau\,\epsilon^2(\tau)/2$, remains constant. We therefore consider the functional optimization of[5,6,9,12]

$$J(t_f)=A(t_f)-\frac{\lambda}{2}\int_{t_0}^{t_f}d\tau\,\epsilon^2(\tau) \tag{11}$$

with respect to the field $\epsilon(\tau)$. The term with the parameter λ (a Lagrange multiplier) is introduced to enforce the energy constraint. The final equation for the optimal weak field can be obtained more directly by recasting the yield $A(t_f)$ [Eq. (6)] in a symmetrized form (see Appendix A)

$$A(t_f)=\frac{1}{2}\int_{t_0}^{t_f}d\tau\int_{t_0}^{t_f}d\tau'\,M^S(\tau,\tau')\epsilon(\tau)\epsilon(\tau'), \tag{12}$$

with the symmetrized material response function, M^S, defined by

$$M^S(\tau,\tau')=M^S(\tau',\tau)\equiv\hbar^{-2}M(t_f-\tau,\tau-\tau'),\quad \tau\geqslant\tau'. \tag{13}$$

Substituting Eq. (12) into Eq. (11), and considering the variational equation $\delta J(t_f)=0$ with respect to a small variation in the field, $\delta\epsilon(\tau)$, we finally obtain the following eigenequation for the optimal weak field[9]

$$\int_{t_0}^{t_f}d\tau'\,M^S(\tau,\tau')\epsilon(\tau')=\lambda\epsilon(\tau). \tag{14}$$

Substituting this equation into Eq. (12), we find that the eigenvalue λ (the Lagrange multiplier) is the yield of our control objective normalized by the incident field energy.[9]

Equation (14) is a homogeneous Fredholm equation[15] and can be recast numerically into a matrix diagonalization by representing the symmetrized material function and the field on discretized time grids. The number of nontrivial solutions to the linear control eigenequation [Eq. (14)] depends on the nature of the target and the molecular system, such as whether it is a pure or mixed state, as well as the complexity and dimension of the molecular dynamics and the Franck–Condon transition. In the general mixed state case, there can be multiple local optimal solutions.[16] The largest eigenvalue of the symmetrized matrix is the *globally* optimal yield, and the eigenfunction corresponding to it is the globally optimal weak electric field.[9]

B. Application to two-state systems

The equations presented so far are general for any material system beginning in a steady state (e.g., in thermal equilibrium). We now specialize the equations to a molecular system with two adiabatic electronic states, $|g\rangle$ and $|e\rangle$, our goal being to control the dynamics on either of the two states in a specified manner. In this case,

$$H_M=H_g|g\rangle\langle g|+(H_e+\hbar\omega_{eg})|e\rangle\langle e|, \tag{15}$$

$$D=\mu[\,|e\rangle\langle g|+|g\rangle\langle e|\,]. \tag{16}$$

Here, H_n is the adiabatic Hamiltonian governing the molecular nuclear dynamics in electronic state $n=g$ or e, μ is the electronic transition dipole moment (depending in general on the molecular nuclear coordinates) which couples the two electronic states, and ω_{eg} is the difference between the potential energy minima of the two states, i.e., $\omega_{eg}=T_e/\hbar$, where T_e is the electronic term value. Since ω_{eg} is usually large compared with the characteristic nuclear frequencies, we will later remove it by applying the rotating wave approximation (RWA). The molecular system is assumed to be initially in a steady state (e.g., in thermal equilibrium or a specified vibronic level) of the ground electronic manifold with

$$\rho(t_0)=\rho_g(t_0=-\infty)|g\rangle\langle g|. \tag{17}$$

The target operator $\hat{A}$ is given by

$$\hat{A}=\hat{A}_n|n\rangle\langle n|,\quad n=g\text{ or }e, \tag{18}$$

where $\hat{A}_n$ is an operator in the nuclear space of the electronic surface n. The yield $A(t_f)$ is then the overlap of $\hat{A}_n$ with either an excited state phase space wave packet (ρ_e) following, e.g., a weak pump field, or a ground state phase space wave packet (ρ_g) created by, e.g., a weak field Raman excitation.

For this two surface model, the material function takes the form

$$M(t_2,t_1)=\begin{cases}2\,\mathrm{Re}\langle D(0)\hat{A}(t_2+t_1)D(t_1)\rangle & \text{if } n=e\\ -2\,\mathrm{Re}\langle\hat{A}(t_2+t_1)D(t_1)D(0)\rangle & \text{if } n=g\end{cases}$$
$$=2\,\mathrm{Re}[M_n(t_2,t_1)\exp(-i\omega_{eg}t_1)]. \tag{19}$$

Thus, the two terms in Eq. (8) can be related to excited and ground state molecular control, respectively. Using the definitions of the operators given above, the material functions specific to excited and ground state control, M_e and M_g, respectively, are found to be

$$M_e(t_2,t_1)=\mathrm{Tr}[\mu_{ge}(0)\hat{A}_e(t_2+t_1)\mu_{eg}(t_1)\rho_g(t_0)] \tag{20}$$

and

$$M_g(t_2,t_1)=-\mathrm{Tr}[\hat{A}_g(t_2+t_1)\mu_{ge}(t_1)\mu_{eg}(0)\rho_g(t_0)], \tag{21}$$

where

$$\hat{A}_n(t)=e^{iH_nt/\hbar}\hat{A}_ne^{-iH_nt/\hbar},\quad \mu_{mn}(t)=e^{iH_mt/\hbar}\mu e^{-iH_nt/\hbar}. \tag{22}$$

For the remainder of this paper, we shall specialize to the case of excited state control via a resonant electronic light-matter interaction and apply the RWA for the weak control field. This approximation is made by neglecting the integration of highly oscillatory contributions due to the electronic transition. We therefore write the light field $\epsilon(t)$ in the form

$$\epsilon(t)=E(t)e^{-i\omega_{eg}t}+E^*(t)e^{i\omega_{eg}t}, \tag{23}$$

where $E(t)$ is a slowly varying complex function, which in general contains a time dependent excess excitation frequency which causes for the molecular nuclear dynamics on the excited state. Substitution of Eqs. (18)–(20) and (23) into Eq. (12) gives an equation for the yield within the RWA (see Appendix A)

$$A(t_f)=\int_{t_0}^{t_f} d\tau \int_{t_0}^{t_f} d\tau'\, M_e^S(\tau,\tau')E^*(\tau)E(\tau'). \tag{24}$$

Here, $M_e^S(\tau,\tau')$ is the symmetrized Hermitian form of M_e [rather than a real symmetric form as in Eq. (13)]

$$M_e^S(\tau,\tau')=[M_e^S(\tau',\tau)]^* \equiv\hbar^{-2}M_e(t_f-\tau,\tau-\tau'), \quad \tau'\leqslant\tau. \tag{25}$$

In Eq. (24), it is not necessary to explicitly take the real part of the right-hand side since the Hermitian nature of M_e^S automatically guarantees that the result is real. As described above [cf. Eq. (14)], we can calculate the globally optimal field from an eigenequation, which for the two-state system discussed here takes the form[9]

$$\int_{t_0}^{t_f} d\tau'\, M_e^S(\tau,\tau')E(\tau')=\lambda E(\tau). \tag{26}$$

If M_e^S and E are represented on discretized time grids, Eq. (26) becomes a conventional matrix eigenvalue equation

$$\mathbf{M}_e^S\mathbf{E}=\lambda\mathbf{E} \tag{27}$$

in which the largest eigenvalue λ is the globally maximal yield, and thus, the corresponding eigenvector is the *globally* optimal field for the control problem.[9] We note that Eq. (26) is valid for the slowly varying envelope of the optimal control field, while Eq. (14) gives the complete non-RWA field. The envelope can be calculated from the diagonalization of a matrix M_e^S which is of much smaller dimension than M^S since a larger time step can be used.

In order to quantify the degree to which the optimal field succeeds in meeting the objective, we define an "achievement function" $\alpha(t)$ by

$$\alpha(t)=\left(\frac{\mathrm{Tr}[\hat{A}_e\rho_e(t)]}{\mathrm{Tr}\,\hat{A}_e\,\mathrm{Tr}\,\rho_e(t_f)}\right)^{1/2}. \tag{28}$$

In Eq. (28), $\rho_e(t)$ is the density matrix (or phase space wave packet) created on the excited state by an arbitrary excitation field $E(t)$ and is given formally by the corresponding matrix element, $\rho_e(t)\equiv\langle e|\rho(t)|e\rangle$, of Eq. (2). This achievement function satisfies the inequality $0\leqslant\alpha(t)\leqslant1$. The value of the achievement function at the target time, $\alpha(t_f)$, is a measure of how well the controlled phase space wave packet, created by the interaction of the molecule with the optimal field, overlaps the desired target, and can be thought of as the normalized expectation value of the target operator over the density matrix $\rho_e(t_f)$.

C. Hilbert–Schrödinger formulation

In the previous subsections, we developed formal expressions for the weak field optimal control of molecular dynamics in a density matrix formulation. These results allow the study of optimal control, e.g., in the presence of solvents and at finite temperatures,[9] as well as prescribing a route to classical and semiclassical treatments. In this subsection, we consider the optimal control of molecular dynamics in the pure state case and recast our previous results in terms of Schrödinger wave-function dynamics in Hilbert space. For clarity, we consider the optimal control of molecular dynamics in the excited electronic state $|e\rangle$, as described in the last subsection. We assume that the molecular system is initially in a vibrational eigenstate $\rho_g(t_0)=|v''\rangle\langle v''|$ in the electronic ground $|g\rangle$ state. In this case, the corresponding unsymmetrized molecular control response function, M_e of Eq. (20), becomes

$$M_e(t_2,t_1)=\langle\psi_e^0(t_2)|\hat{A}_e|\psi_e^0(t_2+t_1)\rangle \tag{29}$$

with $\psi_e^0(0)=\mu|v''\rangle$ and

$$|\psi_e^0(t)\rangle=\exp[-i(H_e-\epsilon_{v''})t/\hbar]\,|\psi_e^0(0)\rangle. \tag{30}$$

In Eq. (30), $\epsilon_{v''}$ is the energy of vibronic level $|v''\rangle$ in the ground electronic $|g\rangle$ state and $|\psi_e^0(t)\rangle$ can be thought as the wave function in the electronic $|e\rangle$ state resulting from a $\delta(t)$ pulse excitation. The true excited wave function $|\psi_e(t)\rangle$ (or $\rho_e(t)=|\psi_e(t)\rangle\langle\psi_e(t)|$) can be obtained by a convolution of $\psi_e^0(t)$ with the electric field $E(t)$

$$\psi_e(t)=\hbar^{-1}\int_{t_0}^{t} d\tau\, E(\tau)\psi_e^0(t-\tau). \tag{31}$$

In concluding this section, we specify the Gaussian control target $\hat{A}_e$, which will be used throughout the remainder of this paper. Consider control of a single mode molecular system, e.g., a diatomic molecule in which we consider only the vibrational coordinate. A general Gaussian target $\hat{A}_e$ can be characterized by a set of five parameters, $\bar{p}$, $\bar{q}$, w_{pp}, w_{qq}, and $w_{pq}(=w_{qp})$, to represent the centers, variances, and phase space orientation of the target wave packet with respect to momentum and position. In the Wigner phase space representation, the target operator $\hat{A}_e$ has the form[9,17]

$$A_W(p,q)\equiv\frac{1}{2\pi\hbar}\int_{-\infty}^{\infty} ds\, e^{-ips/\hbar}A(q+s/2,q-s/2) =\frac{1}{2\pi C}\exp\left(-\frac{1}{2C^2}[w_{qq}(p-\bar{p})^2+w_{pp}(q-\bar{q})^2 -2w_{pq}(p-\bar{p})(q-\bar{q})]\right) \tag{32}$$

with $C\equiv(w_{pp}w_{qq}-w_{pq}^2)^{1/2}$. In Eq. (32), $A(x,x')\equiv\langle x|\hat{A}_e|x'\rangle$ is the target operator in the configuration space representation, which can be obtained by the Fourier transform of the Wigner representation, A_W. We have[17]

$$A(x,x') = (2\pi w_{qq})^{-1/2} \exp[i\bar{p}(x-x')/\hbar] \times \exp\left(-\frac{1}{2w_{qq}} [(x+x'-2\bar{q})^2/4 + (C/\hbar)^2 \times (x-x')^2 - i(w_{pq}/\hbar)(x+x'-2\bar{q})(x-x')] \right). \quad (33)$$

The prefactors in Eqs. (32) and (33) are chosen such that the target wave packet is normalized

$$\mathrm{Tr}\,\hat{A}_e = \int\int dp\,dq\,A_W(p,q) = \int dx\,A(x,x) = 1. \quad (34)$$

The procedure for computing the optimal electric field is now straightforward. One first calculates $\psi_e^0(x,t) = \langle x|\psi_e^0(t)\rangle$ by propagating $\psi_e^0(x,0) = \langle x|\mu|\nu''\rangle$ on the excited state surface, as in Eq. (30). The configuration space form of the target is calculated using Eq. (33) for a specified Gaussian target, and the integral in Eq. (29) is calculated for a square grid of t_1 and t_2 values. The symmetrized version of M_e is then constructed [Eq. (25)] and diagonalized. The largest eigenvalue from this diagonalization is the highest possible yield, and the corresponding eigenvector is the globally optimal electric field. Note that changing the target often only requires performing the overlap integration in Eq. (29) and the diagonalization; the time-consuming calculation of $\psi_e^0(x,t)$ need not be repeated. The excited-state wave function $\psi_e(t)$ in the presence of weak field can then be calculated for any given $E(t)$ via Eq. (31). This field $E(t)$ can be, e.g., the globally optimal field as mentioned above or a parametrized optimal field as discussed in Sec. IV. The achievement function $\alpha(t)$ [Eq. (28)] can be calculated in the wave-function formulation as

$$\alpha(t) = [\langle\psi_e(t)|\hat{A}_e|\psi_e(t)\rangle]^{1/2} = \left(\int dx \int dx'\,\psi_e^*(x,t)A(x,x')\psi_e(x',t) \right)^{1/2}. \quad (35)$$

In this equation, we normalize $\psi_e(t)$ at all times by $[\mathrm{Tr}\,\rho_e(t_f)]^{-1/2} = \langle\psi_e(t_f)|\psi_e(t_f)\rangle^{-1/2}$, the square root of the total population on the excited state at the target time, t_f.

Finally, we specialize to the minimum uncertainty case in which $C = (w_{pp}w_{qq} - w_{pq}^2)^{1/2} = \hbar/2$. In this case, the control target of Eq. (32) is a pure state[17] and its configuration space representation $A(x,x')$ has the form

$$A(x,x') = \Phi(x)\Phi^*(x') \quad (36)$$

with[18]

$$\Phi(x) = (2\pi w_{qq})^{-1/4} \exp\left[-\frac{1-(2i/\hbar)w_{pq}}{4w_{qq}} (x-\bar{q})^2 + i\bar{p}(x-\bar{q})/\hbar \right]. \quad (37)$$

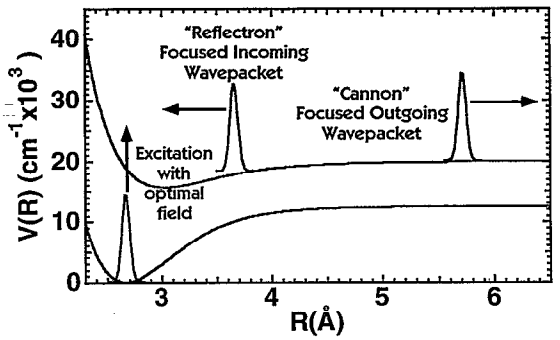

FIG. 1. Potential energy curves for the I_2 ground X and excited B states. The target in configuration space for the molecular cannon and the molecular reflectron are displayed as well. The zero of energy is chosen to be the X state minimum.

The achievement function $\alpha(t)$ [Eq. (35)] can therefore be further simplified as

$$\alpha(t) = |\langle\Phi|\psi_e(t)\rangle| = \left| \int dx\,\Phi^*(x)\psi_e(x,t) \right| \quad (38)$$

which explicitly shows that the achievement function is just the overlap of the target wave function with the molecular state wave function created by the electric field $E(t)$.

III. MOLECULAR CANNONS AND REFLECTRONS

Section II has given the framework for calculating globally optimal weak field control, both in the general case and for the specific case of excited state control in a two-level system. In this section, we apply these methods to three illustrative examples. These examples for simplicity use targets which are minimum uncertainty phase space distributions, as described below, but we emphasize that any target can be expressed as an operator in phase space.

A. A molecular cannon: Focusing of an outgoing continuum I_2 wave packet

In this example, we consider the focusing of a dissociative wave packet at a particular instant of time. We term this process a molecular cannon, because the result will be focusing matter into outgoing projectiles, i.e., the atoms formed from dissociated molecules, having at a particular time a narrow probability distribution (within the uncertainty principle limit) in both interatomic distance and interatomic velocity. As we shall see in the following, the resulting globally optimal weak field [i.e., the eigenfunction solution to Eq. (26) with the largest eigenvalue] for this molecular cannon process is a simple field with an appropriate chirp. A similar, although nonoptimized, scheme to focus continuum wave packets during photodissociation using chirped light pulses has been proposed independently by Heller.[19] We use I_2 as an example, assuming that it is initially in $|\nu''=0\rangle$, the ground vibronic level, and consider only the vibrational coordinate. In Appendix B, we describe the potentials used for the X and B states, which are displayed in Fig. 1. In particular, the difference in en-

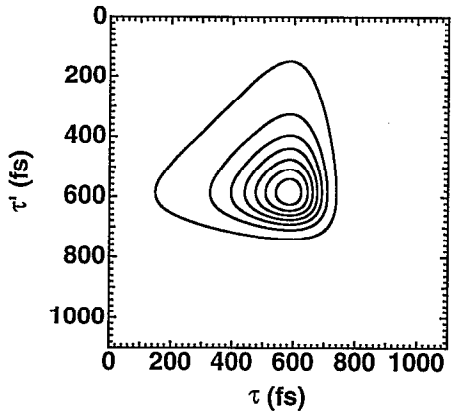

FIG. 2. Amplitude of the symmetrized material response function $M_e^S(\tau,\tau')$ [Eq. (25)] for I_2 cannon excited state control. The upper limits of the time axes are the target time t_f.

ergy between the potential energy minimum of the X state and that of the B state, ω_{eg}, is 15 769 cm^{-1} (Ref. 20). We further, for simplicity, make the Condon approximation and neglect the dependence of the $X \leftrightarrow B$ transition dipole on the internuclear distance and thus assume that μ is constant.

The target for the molecular cannon is defined as a phase space wave packet on the B state centered in position at $\bar{q}=5.84$ Å, with the center of the outgoing momentum, $\bar{p}>0$, corresponding to a kinetic energy, $\bar{p}^2/(2m)$, of 0.05 eV, where m is the reduced mass of I_2. The variances of the target are given by the formulas $w_{qq}=\hbar/(2m\omega)$, $w_{pp}=m\omega\hbar/2$, and $w_{pq}=0$, with $\omega=250$ cm^{-1}. In this case, we have $(w_{pp}w_{qq}-w_{pq}^2)^{1/2}=\hbar/2$ and the target is of minimum uncertainty, as described by Eqs. (36) and (37). The mean energy of this target, relative to the zero of the B state potential energy curve, is $\mathrm{Tr}[\hat{A}H_B]=4720$ cm^{-1}, compared to the B state dissociation energy of 4381 cm^{-1}. The target time t_f is chosen to 1100 fs.

In Fig. 2, we show the amplitude in the time domain of the symmetrized material function, M_e^S [Eqs. (25) and (29)] for the molecular I_2 cannon. This function consists of a single broad peak. Thus, we expect an optimal electric field consisting of a single pulse, and Fig. 3 shows that this is indeed the case. The optimal field is a single pulse with a full width at half-maximum (FWHM) of ~225 fs. This pulse is clearly not a simple Gaussian since it is not symmetric. We will return to a consideration of parametrizing the functional form of this pulse in the next section.

To show both the temporal and frequency structure of the optimal field more clearly, we use a Wigner transform of $E(t)$

$$F_W(t,\omega)=2\,\mathrm{Re}\int_0^\infty d\tau\, e^{-i\omega\tau}E^*(t+\tau/2) \times E(t-\tau/2)W(\tau), \tag{39}$$

where $W(\tau)$ is a window function that reduces the interference normally present in the standard Wigner transform, in which $W(\tau)=1$.[12,21] For the cannon, we employ a

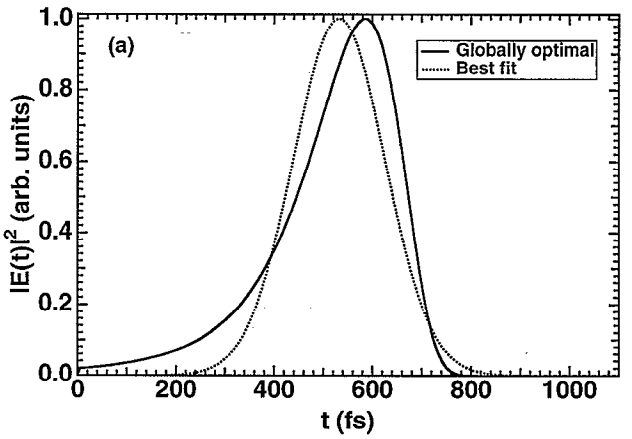

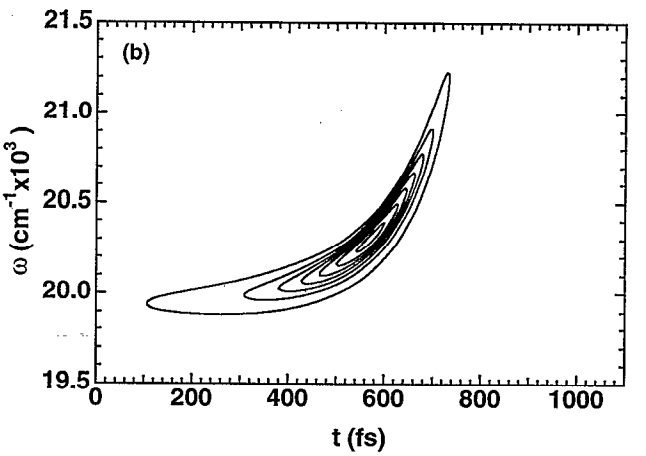

FIG. 3. Globally optimal electric field for I_2 cannon excited state control obtained by diagonalizing M_e^S in Fig. 2. (a) Intensity $|E(t)|^2$ for the globally optimal field. The intensity for the best-fit field, as described in Sec. IV, is also shown (dotted line). The units of the intensity are arbitrary as long as the weak field limit applies. (b) Wigner representation calculated from Eq. (39) with a correlation time τ_c of 70 fs.

Gaussian window function of the form $W(\tau)=\exp(-\tau^2/\tau_c^2)$, where τ_c is a correlation time taken to be on the order of the pulse width. One can show that the effect of this window function is to act as a filter in the frequency domain as well as in the time domain such that interference effects which span a time longer than τ_c are suppressed. [We note that the window function $W(\tau)$ does alter the spectral bandwidth of the pulse. However, for pulses with significant chirps such as the one shown here, the effect is not dramatic.] The Wigner transform of the cannon optimal field is displayed in Fig. 3(b). The time-frequency structure of the globally optimal field reveals a significant positive chirp, the average frequency increasing with time. A sizable linear chirp is seen in the figure, and there is certainly a quadratic chirp present as well, visible as a parabolic curvature of the pulse. The pulse has a rather wide bandwidth, ranging from just above the B state dissociation energy (~20 000 cm^{-1}) to energies greater than 21 000 cm^{-1}. Note that the spectral bandwidth for the intensity of a transform-limited 225 fs pulse is only 65 cm^{-1}, so the extra bandwidth of the optimal field again

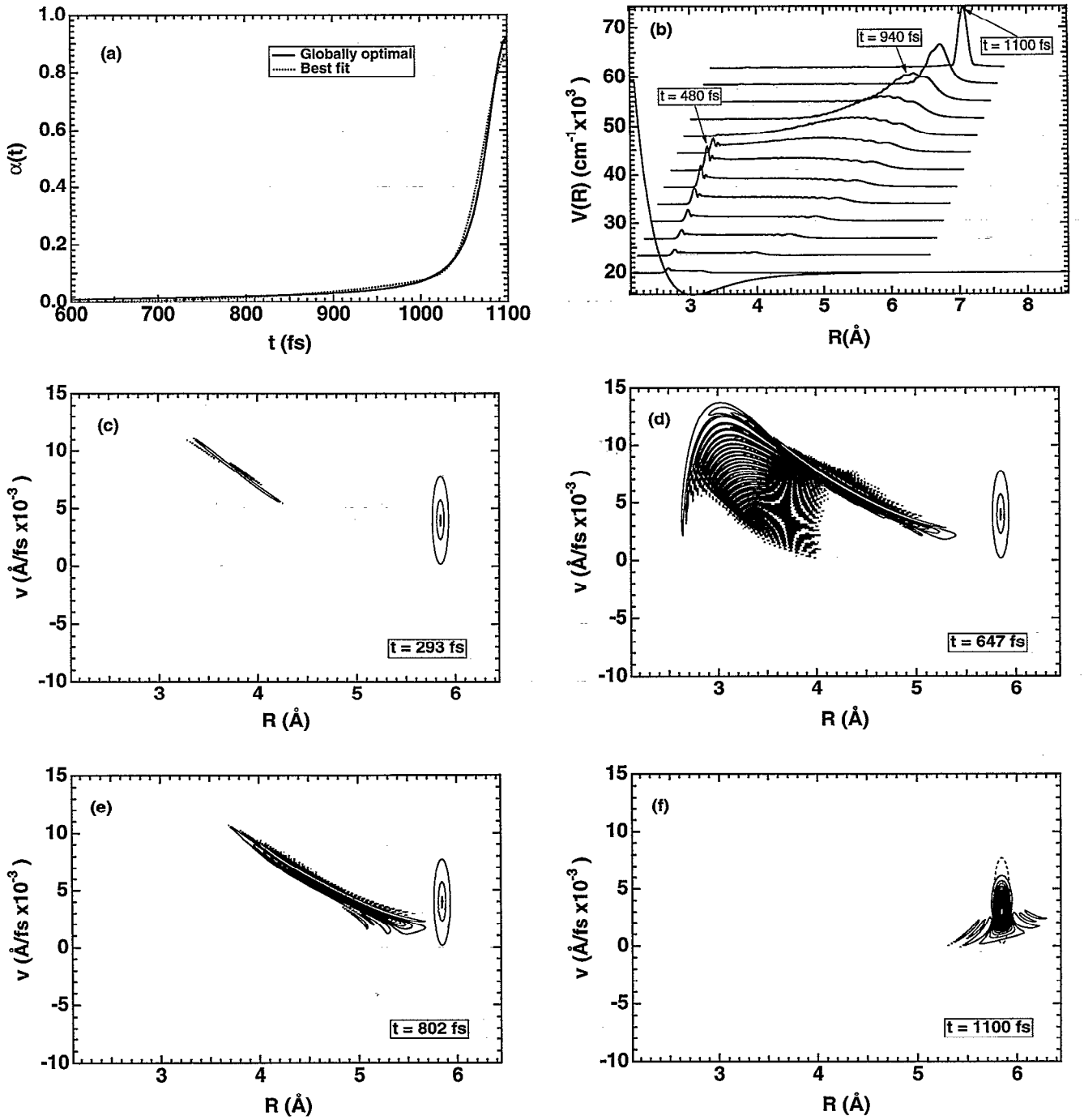

FIG. 4. (a) Achievement function $\alpha(t)$ [Eq. (28)] for the cannon globally optimal field shown in Fig. 3. The achievement function for the best-fit field calculated as described in Sec. IV is also shown (dotted line). Only the last 500 fs of the time duration is shown; for earlier times, $\alpha(t) \cong 0$. (b) Configuration space wave function $\psi_e(R,t)$ showing the dynamics of the molecule under the influence of the globally optimal field. The remaining panels show the time-dependent density matrix $\rho(v,R,t)$ as calculated from the Wigner representation of the configuration space wave functions of (b). To clarify the physical interpretation, we display the density matrix as a function of internuclear velocity rather than momentum. The times at which ρ is plotted are (c) 293 fs, (d) 647 fs, (e) 802 fs, (f) 1100 fs. In panels (c)–(f), the phase space target $A(v,R)$ is also shown.

implies the presence of a substantial frequency chirp.

The achievement function, $\alpha(t)$ [Eqs. (28) or (38)], for the globally optimal field is shown in Fig. 4(a). The achievement is near zero for most of the pulse, and then rapidly rises to its final value of 0.92 over the final 100 fs. The reason for this is clearly evident from Fig. 4(b), where we plot the wave packet, $\psi_e(R,t)$, created by the optimal field. While the field is on, a very broad wave packet is created at small values of R. After the pulse ends, this broad wave packet propagates freely to larger R and progressively narrows until a large overlap with the target is reached at the target time. The Wigner phase space representation of this wave packet, shown in Figs. 4(c)–4(f), gives a similar picture. This representation is defined by

$$\rho(p,q,t)=\frac{1}{2\pi\hbar}\int_{-\infty}^{\infty} ds\, e^{-ips/\hbar}\tilde{\rho}(q+s/2,q-s/2,t), \tag{40}$$

where $\tilde{\rho}$ is the density matrix in configuration space, which for a pure state $\psi(x,t)$ is given by

$$\tilde{\rho}(x,x',t)=\psi_e(x,t)\psi_e^*(x',t). \tag{41}$$

In the Wigner representation, one can see not only the breadth of the packet in configuration space, but also the breadth in momentum space as well. Further, the projections of the Wigner representation on either the p or q axis give information about the wave function in configuration or momentum space, respectively. More explicitly,

$$\int dp\, \rho(p,q,t)=|\psi_e(q)|^2 \tag{42}$$

$$\int dq\, \rho(p,q,t)=|\tilde{\psi}_e(p)|^2, \tag{43}$$

where $\tilde{\psi}_e(p)$ is the wave function in momentum space and can be calculated from the Fourier transform of $\psi_e(q)$. Figure 4(c) shows $\rho(p,q)$ at an early time in the dynamics, shortly after the field has been turned on. One can see that even at this initial stage, substantial spreading in both position and momentum has taken place. As the field continues to excite amplitude to the excited state, the wave packet spreads even more, as shown in Fig. 4(d), and develops considerable interference. After the field is turned off, the higher energy (and momentum) components begin to catch up with the lower energy components that were created at earlier times, as can be seen in Fig. 4(e). As the phase space wave packet approaches the target time, the widths in both configuration and momentum begin to narrow, the interference begins to disappear, and the optimal overlap with the target phase space wave packet is achieved [Fig. 4(f)]. Thus, quantum control has reversed the natural tendency of a quantum wave packet to spread, permitting the focusing of matter at a chosen time into nearly a minimum uncertainty wave packet centered at a chosen position and momentum.

An approximate classical picture of the physics involved in this process can also be divined. We have formulated the problem such that the molecule has a certain amount of time to create an unbound continuum wave packet at a particular center position with a particular center momentum. The lower energy (and momentum) components of the continuum wave packet will take relatively longer times to reach the position of the target, and the higher energy components will take shorter times. Thus, to achieve the maximum overlap with the target, a pulse with a substantial positive chirp is required so that the higher frequencies in the pulse arrive at later times. In fact, that is exactly what we find in this case, as Fig. 3(b) shows. Classical mechanics cannot, of course, account for the interference visible in Fig. 4. We are currently analyzing the effects of this interference on the dynamics to see under what circumstances, if any, a classical implementation of the control equations is adequate to predict the optimal field.

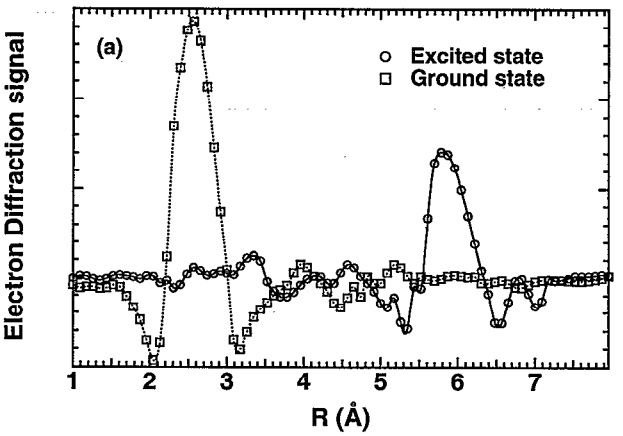

FIG. 5. Simulation of I_2 molecular cannon by ultrafast electron diffraction with 2×10^7 detected electrons. The simulated signal is shown after transformation to coordinate space.

To conclude our discussion of the cannon, we consider the experimental observation of the focused state. Techniques such as ultrafast pump-probe and pump-dump spectroscopy, which will be useful for the two systems we describe below, are not as likely to be effective for the cannon. When the internuclear separation is large, it is difficult to characterize the focused wave packet by the conventional techniques of molecular spectroscopy because the Franck–Condon overlaps with nearby electronic states will be poor. Thus, only the atomic spectra of the fragments are observable, and, unfortunately, these spectra will not show a strong dependence on the internuclear separation at large separations.

However, the substantial difference between the internuclear distance on the initial ground electronic state and the distance at which focusing takes place on the excited electronic state can in principle be detected by ultrafast electron[22,23] and x-ray diffraction.[24,25] We illustrate this effect in preliminary simulations of electron scattering from the I_2 molecular cannon, as shown in Fig. 5. The simulations were performed for the ground state and for the time-evolved wave packet at the final time t_f. In these simulations, it was assumed that the electrons were energetic (Born approximation) and that the atomic scattering factors are valid for the molecule. The time duration of the electron pulse was ignored. Monte Carlo sampling was employed to average over the orientation of the molecule. These calculations are meant to be illustrative of the qualitative trends that can be expected in experiments, and not to make detailed predictions of experimental results; however, they do indicate that it may be possible to observe the focused wave packet with ultrafast diffraction. The simulation of ultrafast x-ray diffraction experiments gives similar results. More accurate calculations are underway and will be reported in future work.[26] Ultrafast spectroscopy and diffraction experiments are under development in our laboratory[26,27] to detect quantum control of molecular dynamics such as in the examples discussed in this paper.

B. A molecular reflectron: Focusing of an incoming wave packet of I_2

In the previous section, we demonstrated the focusing of an unbound outgoing wave packet. We will now show that bound incoming wave packets can be focused as well. This process is analogous to a charged particle reflectron in which a reflecting potential is designed to focus a pulse of ions or electrons of known properties. In the molecular reflectron we describe here, the potential on which the matter pulse moves is known and fixed, and so the objective is to find the electric field that produces a time-dependent matter pulse which is focused at a chosen time about a particular position and momentum. Once again, we study as an example the I_2 $B \leftarrow X$ ($v''=0$) transition. In this case, though, the target wave packet on the B surface is centered in position at $\bar{q}=3.72$ Å and has an incoming momentum centered at $\bar{p}<0$, corresponding to a kinetic energy of $\bar{p}^2/(2m)=0.05$ eV. The variances of the target phase space wave packet are chosen to be the same as in the cannon case and the target time is set to $t_f=550$ fs. This problem is sufficiently similar to the cannon that we only present a brief description of the results, highlighting the differences between the reflectron and the cannon.

The amplitude of the material function M_e^S for this problem shows essentially the same single pulse structure of its cannon counterpart. Similarly, the optimal electric field for this problem consists of a single pulse of ~ 100 fs FWHM duration, as displayed in Fig. 6(a). The Wigner transform of the field, as shown in Fig. 6(b), has the same basic structure as that of the cannon, with two significant differences. First, the center frequency of the reflectron pulse is ~ 2000 cm^{-1} less than that for the cannon. Thus, the reflectron operates within the bound vibrational levels of the I_2 B state. The mean energy of the reflectron target, as measured from the zero of the B state, is $\mathrm{Tr}[\hat{A}H_B]$ $=2867$ cm^{-1}, which is 1853 cm^{-1} lower than that of the cannon target and lower than the B state dissociation energy by 1514 cm^{-1}. Second, Fig. 6(b) shows a negative chirp for the reflectron pulse, contrasting with the positive chirp for the cannon pulse.

The achievement function, $\alpha(t)$, for the reflectron pulse is similar to that for the cannon. The value of the achievement for the reflectron at t_f is 0.97. However, the evolution of the configuration space wave packets, as displayed in Fig. 7, shows that there is a different mechanism operating in the reflectron. The wave packet reflects off the softer outer wall at large internuclear distances, and then focuses shortly thereafter on the return trip. The phase space picture shows that the wave packet at the target time t_f does indeed have significant negative momentum.

The chirp of the globally optimal field for the reflectron has the opposite sign of that for the cannon globally optimal field. The negative chirp means that the higher energy components of the wave packet on the B state are created first for the reflectron, while the lower energy components actually take a *shorter* time to reach the target state. The reason for this behavior is that the higher energy states in the anharmonic excited state potential correspond to longer vibrational periods. Since essentially all components of the reflectron wave packet are bound, the higher energy portion accesses flatter regions of the B state potential, where the forces are smaller, so that the wave packet spends a longer time with low velocity before reflecting. This is in direct contrast to the continuum cannon wave

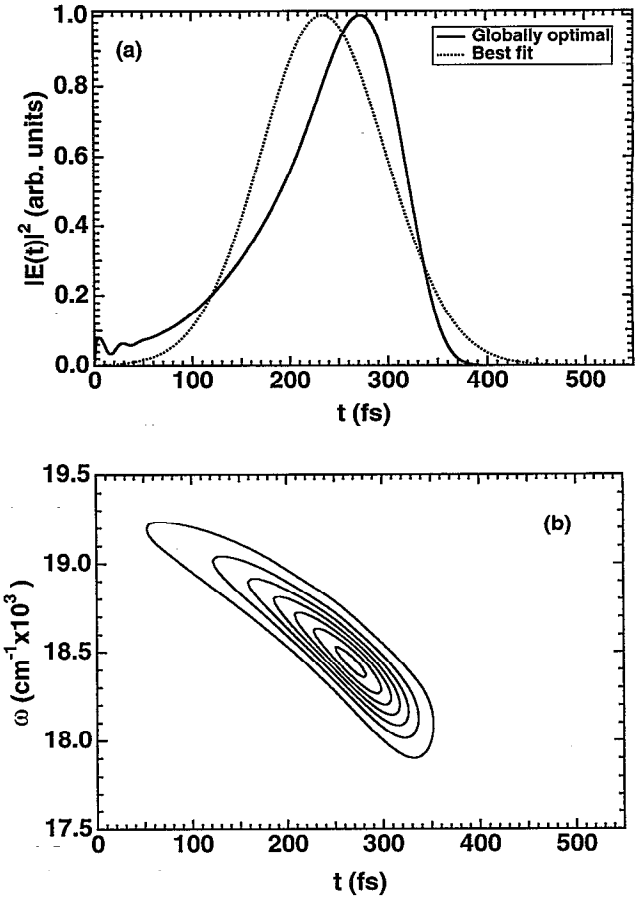

FIG. 6. Globally optimal electric field for I_2 reflectron excited state control. (a) Intensity $|E(t)|^2$ of the globally optimal field. The intensity for the best-fit field, as described in Sec. IV, is also shown (dotted line). (b) Wigner representation calculated from Eq. (39) with a correlation time τ_c of 35 fs.

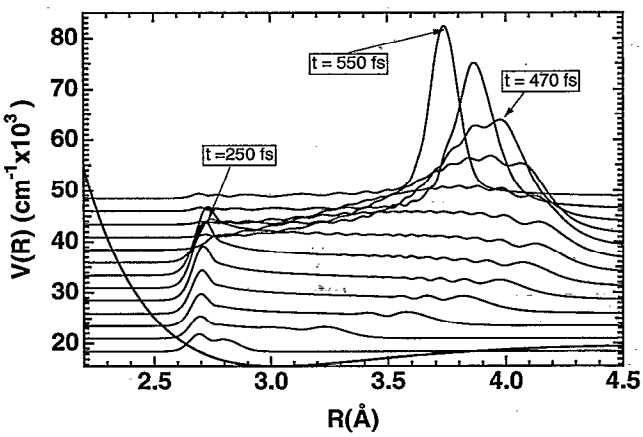

FIG. 7. Configuration space wave function $\psi_e(R,t)$ showing the dynamics of the molecule under the influence of the globally optimal field.

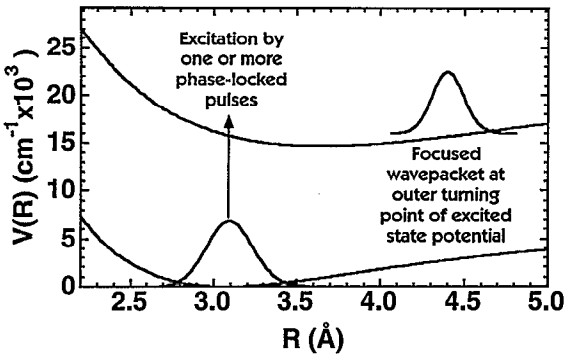

FIG. 8. Potential energy curves for the Na_2 ground X and excited A states. The configuration space form of the target is displayed. The zero of energy is chosen to be the X state minimum.

packet where turning points do not have an important effect. Therefore, for the reflectron, the higher energy portions of the wave packet, which take longer to return to the target area, must be created earlier than the lower energy portions. It is important to emphasize that none of this information is built into the process of solving for the optimal field. The theory described above automatically finds the globally optimal field, sometimes with unexpected results, and it is then up to us to understand the physical mechanism by which the optimal field operates.

C. Focusing of a bound state wave packet of Na_2

For our third example, we focus a wave packet on the excited A state of Na_2 in the bound region of phase space at a turning point of the potential. The potential energy curves for the two states of Na_2 are modeled as Morse potentials calculated from the experimental parameters listed by Bardsley *et al.*[28] and are plotted in Fig. 8. In this system, ω_{eg} is equal to 14 680.4 cm^{-1}. Again, we assume that the molecule is initially at the $v''=0$ of the ground electronic state and set the transition dipole moment equal to one. The target wave packet is chosen to have an average momentum of zero and its position is centered at 4.46 Å. The variances of the target are calculated using $\omega=122$ cm^{-1}, and the target is of minimum uncertainty. The average energy of the target, measured with respect to the zero of the A state potential energy surface is 1132 cm^{-1}. The target time t_f is set to 900 fs.

The symmetrized material function for this system shows 3×3 peaks, corresponding to an optimal electric field of three pulses. The actual optimal electric field does indeed contain three pulses, as Fig. 9(a) shows. In the time domain, the three pulses become progressively narrower, and are separated by ~295 fs, corresponding to the vibrational period of the target on the A potential surface at the target energy. (Three pulses is the maximum number that can be supported by the chosen duration of the interaction, $t_f-t_0=900$ fs, assuming that the pulses are separated by the vibrational period of 295 fs.)

For the globally optimal Na_2 field, we construct a Wigner transform using a Gaussian weight function $W(t)$, as in the cannon and the reflectron. The Wigner transform

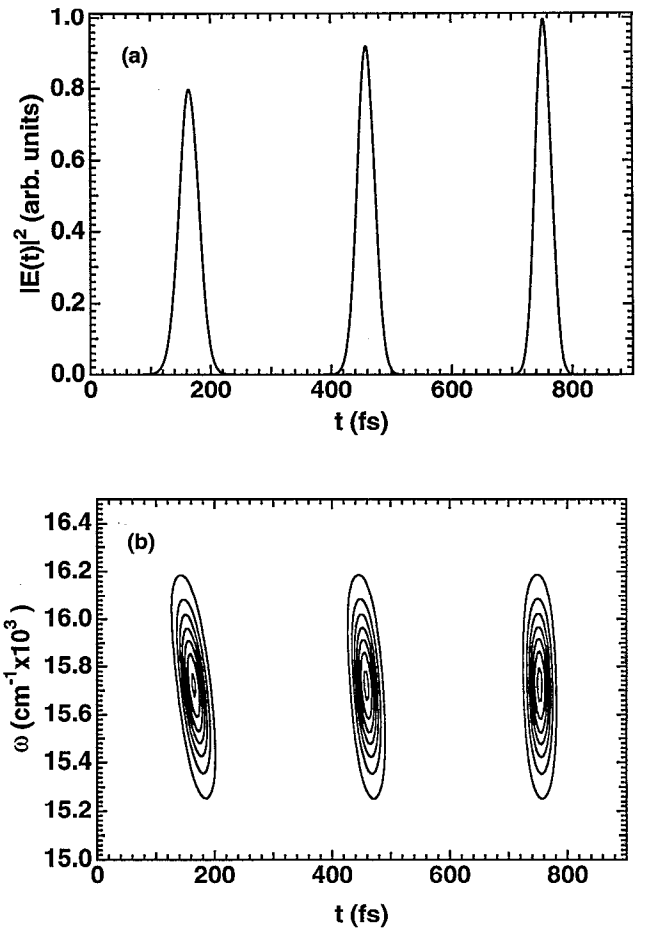

FIG. 9. Globally optimal electric field for Na_2 excited state control. (a) Intensity $|E(t)|^2$ of the globally optimal field. The intensity for the best-fit field, as described in Sec. IV, is identical on the scale of this figure. (b) Wigner representation calculated from Eq. (39) with a correlation time τ_c of 58 fs.

of the globally optimal field, as displayed in Fig. 9(b), shows a simple structure in which the center of each pulse in both frequency and time, the temporal widths, and the frequency bandwidths can be easily seen. From this figure, we note that the temporal widths of the pulses become progressively smaller, and that the size of the chirp (i.e., the amount of change in the frequency distribution during the pulse) also decreases in successive pulses. These three pulses are phase locked, which results in mutual coherent interference in the standard Wigner transform. By setting the correlation time τ_c in the Wigner transform to be sufficiently long, we have, for clarity, suppressed the interference among the three pulses.

The achievement function $\alpha(t)$ for this system, as defined in Eq. (28) and calculated from Eq. (35), shows there are three peaks, corresponding to the three sequential pulses in the optimal electric field, and that the final value of the achievement is 0.98. The intensities of the three peaks are in the approximate ratio of 1:4:9, arising from amplitude ratios of 1:2:3 due to constructive interference of the wave packets created by the three light pulses. This ratio would be exact if the ground and excited state poten-

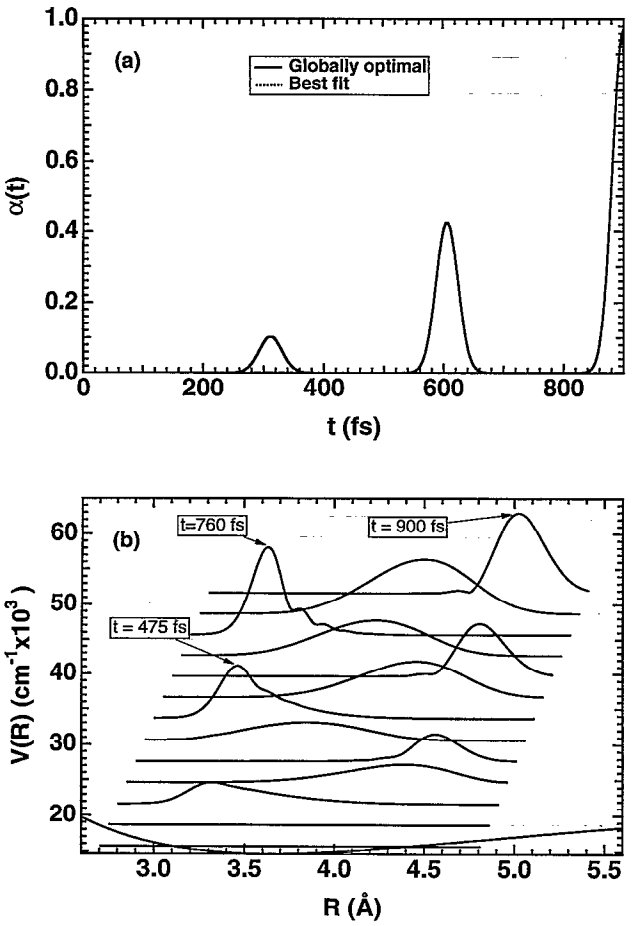

FIG. 10. (a) Achievement function $\alpha(t)$ [Eq. (28)] for the Na_2 globally optimal field shown in Fig. 9. The achievement function for the best-fit field calculated as described in Sec. IV is also shown (dotted line). (b) Configuration space wave function $\psi_e(R,t)$ showing the dynamics of the molecule under the influence of the globally optimal field.

tials were harmonic oscillators.[9] The use of phase-locked pulses to create constructive interference of this type has been demonstrated experimentally by Scherer, Fleming and co-workers.[4] Figure 10(b) shows the evolution of the time-dependent wave function in coordinate space for this process, illustrating that amplitude is transferred to the excited state by the constructive interference of the three pulses. Such constructive interference is an effective method for reaching the selected target and, as this globally optimal field shows, the chirps can be chosen to negate the effects of the spreading of the wave packet.

IV. TOWARD EXPERIMENTALLY REALIZABLE LIGHT FIELDS: FITTED AND OPTIMIZED PARAMETRIZED FIELDS

The techniques described above allow a straightforward calculation of the globally optimal fields, in the weak field limit, that give the optimal overlap with targets defined in phase space. Experimentally, however, light fields can only be produced within a restricted universe of feasible fields. In this section, we will show that by describing this experimentally accessible universe of light fields by an equation with variable parameters, we can either fit the globally optimal unrestricted field by the parametrized form, or find the experimental field within the parametrized universe which maximizes the yield. The simple structure of the globally optimal fields described in the previous section suggests that simple functional forms will be successful in representing these fields. Fits to a parametrized description of the optimal electric field have also been discussed by Rice and co-workers[29] and Somloi and Tannor[13] for the control of I_2 photodissociation yields.

We choose for illustrative purposes to parametrize the light field as a coherent superposition of chirped Gaussian pulses with the following form:

$$E(t)=\sum_j E_j(t), \tag{44}$$

where

$$E_j(t)=A_j \exp[-(t-\bar{t}_j)^2/(2\Gamma_j^2)]\exp[-i\varphi_j(t)]. \tag{45}$$

The phase function $\varphi_j(t)$ can be expanded in a Taylor series to give

$$\varphi_j(t)=\sum_{n=0}^{\infty}\frac{1}{n!}\frac{\partial^n\varphi_j(t)}{\partial t^n}\bigg|_{t=\bar{t}_j}(t-\bar{t}_j)^n. \tag{46}$$

We keep the first four terms of Eq. (46), and denote the time derivatives of $\varphi(t)$ by simpler coefficients to give

$$\varphi_j(t)=\bar{\varphi}_j+\bar{\omega}_j(t-\bar{t}_j)+\tfrac{1}{2}c_j'(t-\bar{t}_j)^2+\tfrac{1}{6}c_j''(t-\bar{t}_j)^3. \tag{47}$$

This procedure results in a time dependent frequency given by

$$\omega_j(t)\equiv\dot{\varphi}_j(t)=\bar{\omega}_j+c_j'(t-\bar{t}_j)+c_j''/2(t-\bar{t}_j)^2. \tag{48}$$

Thus, each pulse $E_j(t)$ has amplitude A_j, mean phase $\bar{\varphi}_j$, temporal center $\bar{t}_j$, and excess carrier frequency $\bar{\omega}_j$. We note that the true carrier frequency is $\omega_{eg}+\bar{\omega}_j$, [cf. Eq. (23)], in which ω_{eg} is the frequency corresponding to the difference in energies between the potential energy minima of the ground and excited electronic states. The second- and third-order terms of the Taylor series expansion of $\varphi_j(t)$ allow for the possibility of chirp through the linear chirp parameter c_j' and the quadratic chirp parameter c_j''. The temporal FWHM of the pulse is independent of the phase and thus of the chirp and is given by $T_{\mathrm{FWHM}}=(\ln 16)^{1/2}\Gamma_j$. In the unchirped or transform-limited case ($c_j'=c_j''=0$), the FWHM in the spectral domain is given by $\Omega_{\mathrm{FWHM}}=\ln 16/T_{\mathrm{FWHM}}$. One can choose other functional forms for the individual pulses,[30] and the methods described below will be equally applicable.

The functional form for the light field described above requires seven parameters for each component pulse. In order to determine the success of this functional form in representing the globally optimal fields, we fit the unrestricted optimal fields of the previous section by Eqs. (44)–(47). As we expect, the field constructed from such a fit does not give as high a yield as that of the unrestricted

TABLE I. Best-fit Gaussian pulse parameters for I_2 molecular cannon optimal field.

Parameter	Best-fit value
A	1.0
$\bar{t}$	532 fs
Γ	130 fs (T_{FWHM}=220 fs)
$\bar{\varphi}$	...
$\bar{\omega}+\omega_{eg}$	20 200 cm^{-1}
c'	2.3 $\mathrm{cm}^{-1}/\mathrm{fs}$
c''	$1.3\times10^{-2}\mathrm{cm}^{-1}/\mathrm{fs}^2$

globally optimal field, although as we shall show it still does very well for the cases considered here.

A. Nonlinear fit

The fit of the unrestricted field by the functional form described above is performed as follows.

(1) The temporal amplitude of the field, $|E(t)|$, is used for an initial fit of the parameters A_j, $\bar{t}_j$, and Γ_j for a specified number of pulses. Initial guesses for these parameters for this portion of the fit can be estimated directly from plots such as Fig. 9(a).

(2) The parameters calculated in (1) are held fixed, and the phase parameters $\bar{\varphi}_j$, $\bar{\omega}_j$, c_j', and c_j'' are fit for each field $E_j(t)$ separately. The initial guesses for the phase $\bar{\varphi}_j$ are chosen as the phase of the pulse at the center time t_j. The initial guesses for $\bar{\omega}_j$ and the linear chirp can be found directly from the power spectrum of the jth pulse, $|\hat{E}_j(\omega)|^2$, where

$$\hat{E}_j(\omega)=(2\pi)^{-1/2}\int_{-\infty}^{\infty} dt\, e^{i\omega t}E_j(t). \tag{49}$$

In the absence of the quadratic chirp ($c_j''=0$), the power spectrum of the jth field, $|\hat{E}_j(\omega)|^2$, is a Gaussian with center frequency $\bar{\omega}_j$ and width $\Omega_{\mathrm{FWHM}}=(\ln 16)^{1/2}\Gamma_j^{-1}[1+(c_j'\Gamma_j^2)^2]^{1/2}$. This equation can be solved to give the initial guess for the linear chirp, c_j'. The initial guess for the quadratic chirp is chosen to be 0, and the initial guess for $\bar{\omega}_j$ is the FWHM of $\hat{E}_j(\omega)$.

(3) With the results from (1) and (2) as an initial guess, the full field is fitted, allowing all seven parameters to vary.

The nonlinear fit is performed using a standard implementation of the Levenberg–Marquardt method (nonlinear least-squares fitting)[31] modified to handle a complex function of real parameters.

B. Results

1. I_2 cannon

The parameters for the best fit to the I_2 molecular cannon globally optimal field are given in Table I, and a plot of the amplitude of the corresponding field is shown in Fig. 3(a). For this field, we see that the best fit does not appear to be a particularly good representation. A single Gaussian pulse is clearly unable to reproduce the asymmetry of the globally optimal field. The difference between the globally optimal and best fit fields appears less dramatic when considering the Wigner representations shown in Figs. 3(b) and 11. A substantial chirp is obvious in both plots, and the parameters of Table I show that both the linear and quadratic chirps are important.

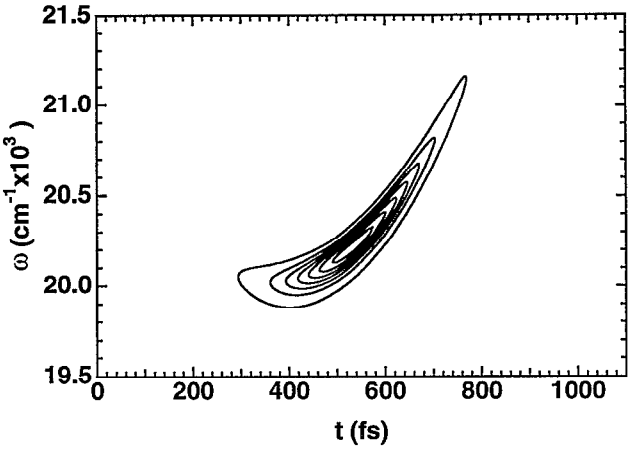

FIG. 11. Wigner representation of the best fit of the globally optimal field by a Gaussian [Eqs. (45)–(47) and Table I] for the I_2 molecular cannon.

As measured by the achievement function, which is shown in Fig. 4(a), the relative yield of the best-fit field is quite good. The best-fit field gives an achievement which is 94% that of the globally optimal field. This result is an indication of the robustness of the globally optimal solution, in that it is not necessary to reproduce perfectly the globally optimal field in order to obtain substantial control over the molecular dynamics. For the cannon, the success of the best-fit results suggests that it is important that the field reproduce the linear chirp of the optimal field, while the exact frequency bandwidth of the field at any given time (which varies significantly over the duration of the optimal field) is not as critical. The importance of the chirp, as evident from an analysis of the best-fit field, is in accord with our qualitative classical description of the physics of the molecular cannon in the previous section.

2. I_2 reflectron

The parameters for the best fit to the globally optimal field for the reflectron are presented in Table II. The primary difference, as we have discussed in the previous section, is that the linear chirp is negative for the reflectron, but of the same order of magnitude as the linear chirp for

TABLE II. Best-fit Gaussian pulse parameters for I_2 molecular reflectron optimal field.

Parameter	Best-fit value
A	1.0
$\bar{t}$	235 fs
Γ	90 fs (T_{FWHM}=150 fs)
$\bar{\varphi}$	...
$\bar{\omega}+\omega_{eg}$	18 580 cm^{-1}
c'	-4.3 $\mathrm{cm}^{-1}/\mathrm{fs}$
c''	-1.1×10^{-2} $\mathrm{cm}^{-1}/\mathrm{fs}^2$

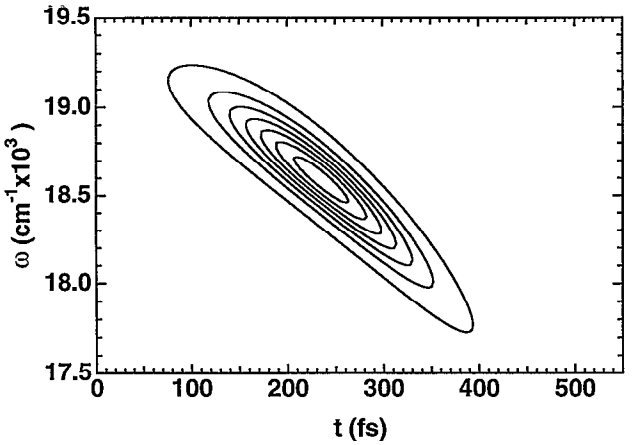

FIG. 12. Wigner representation of the best fit of the globally optimal field by a Gaussian [Eqs. (45)–(47) and Table II] for the I_2 molecular reflectron.

the cannon. This is not surprising, since the magnitude of the chirp is related to the slope of the excited potential in the Franck–Condon region. In Fig. 6(a), we display the best-fit Gaussian field for the reflection problem. As with the cannon, a Gaussian is not a perfect representation of the amplitude of the optimal field. However, in examining the Wigner representation of the best-fit field, as shown in Fig. 12, we find that the overall structure is again similar to the globally optimal solution, although the spectral width at any given time does differ noticeably. The achievement function for the best-fit field shows, however, that the best-fit field is able to create a wave packet that overlaps the target almost as effectively as the optimal field, giving a final achievement of 97% of the achievement of the globally optimal field. As with the cannon, the ability of the parametrized field to reproduce the chirp appears to be a critical factor.

3. Na_2 wave-packet focusing

The parameters for the fit of the Na_2 globally optimal field shown in Fig. 9(a) are presented in Table III. The fit to the globally optimal field is excellent, and shows no significant differences either in intensity or in the Wigner time-frequency representation from the globally optimal field on the scale of the plots in Fig. 9. Figure 10(a) shows that the achievement functions for the globally optimal and best-fit fields are almost identical. The final achievement of the best-fit field, as defined by $\alpha(t_f)$, is 99.95% that of the globally optimal field. Such agreement indicates that the Gaussian pulses are an excellent representation of the globally optimal field in the Na_2 system. This result is not surprising, since the region of the Na_2 potential sampled is very close to harmonic.

As in the preceding cases, the parametrized fit to the optimal field is a convenient description of the properties of the field. In particular, the parameter values confirm several observations that can be made from the plots of the globally optimal field shown in Fig. 9. The three phase-locked pulses do become successively narrower (from the FWHM of 39 fs in the first pulse to 31 fs in the final pulse). The absolute values of the negative linear chirps in the three pulses also successively decrease. The quadratic chirps are positive, as shown in Table III, and have little effect on the field, due to the short duration of the pulses.

The ratio of 1:4:9 of the peaks in the achievement function for the Na_2 wave-packet focusing is indicative of the same type of coherent addition of amplitude on the upper state seen in our previous work on the shifted harmonic oscillator system.[9] The three phase-locked pulses have approximately the same area,[32] $\int dt|\mu E_j(t)/\hbar| \propto A_j\Gamma_j$, as can be calculated from the parameters in Table III. This implies that each pulse creates the same amplitude on the excited potential surface. The maximum achievement can be reached only if the newly created amplitude interferes constructively with the portion that has been created by the previous pulse or pulses. As in the harmonic oscillator system,[9] and as seen in experiment,[33] complete constructive interference requires a sequence of phase-locked pulses. However, unlike the harmonic potential, the Na_2 potential on which the wave packets move is slightly anharmonic. Thus, a wave packet created on the upper state does not return to exactly its original form after traversing the potential. A proper negative chirp, as discussed in the reflectron case, is required to compensate for the dispersion of the wave packet. This chirp allows the wave packet at the inner turning point to interfere nearly perfectly constructively with the amplitude brought to the excited state by the next pulse. The globally optimal weak field, which is found naturally by the theory we have presented, automatically produces the phase locking and chirp, allowing the maximum weak field achievement to be realized.

TABLE III. Best-fit Gaussian pulse parameters for Na_2 optimal field.

Parameter	Pulse 1	Pulse 2	Pulse 3
A_j	0.78	0.91	1.0
$\bar{t}_j$	164 fs	459 fs	753 fs
Γ_j	23 fs (T_{FWHM}=39 fs)	20 fs (T_{FWHM}=34 fs)	19 fs (T_{FWHM}=31 fs)
$\bar{\varphi}_j$	0°	51°	100°
$\bar{\omega}_j+\omega_{eg}$	15 713 cm^{-1}	15 713 cm^{-1}	15 713 cm^{-1}
c_j'	-7.9 $\mathrm{cm}^{-1}/\mathrm{fs}$	-6.5 $\mathrm{cm}^{-1}/\mathrm{fs}$	-2.6 $\mathrm{cm}^{-1}/\mathrm{fs}$
c_j''	$1.2\times10^{-2}\mathrm{cm}^{-1}/\mathrm{fs}^2$	$1.9\times10^{-2}\mathrm{cm}^{-1}/\mathrm{fs}^2$	$1.9\times10^{-2}\mathrm{cm}^{-1}/\mathrm{fs}^2$

C. Nonlinear optimization

While the nonlinear fitting procedure we describe above gives us a good representation of the unrestricted field in the parameter space of Gaussian pulses, there is no guarantee that the resulting set of parameters is that set which gives the maximum yield. To find the maximum yield possible within our parametrized functional space, it may be necessary, especially when we move beyond the weak field limit, to optimize the *yield* with respect to variation of the parameters, using the results of the nonlinear fit as our initial guess for the parameters.

Such an optimization is straightforward to carry out. We first define a yield function that depends on the parameters of the field, which we designate $A(t_f;\boldsymbol{\beta})$, where $\boldsymbol{\beta}$ represents the set of parameters used to define the field. Therefore, we may rewrite Eq. (24) as

$$A(t_f;\boldsymbol{\beta}) = \int_{t_0}^{t_f} d\tau \int_{t_0}^{t_f} d\tau'\, M_e^S(\tau,\tau') E^*(\tau;\boldsymbol{\beta}) E(\tau';\boldsymbol{\beta}). \tag{50}$$

Our goal is then to search the space of parameters $\boldsymbol{\beta}$, such that they maximize $A(t_f;\boldsymbol{\beta})$ under the constraint that the total incident field energy remains constant. This constraint forces us to work in a parameter space that does not allow the amplitudes of the constituent pulses to increase without limit. To do this, we impose a constraint on the energy of the field of the form

$$\int_{t_0}^{t_f} d\tau |E(\tau;\boldsymbol{\beta})|^2 = 1. \tag{51}$$

The imposition of this constraint is performed through a quadratic penalty function, so that the function of the parameters $\boldsymbol{\beta}$ that we maximize is [cf. Eq. (11), noting that $\int d\tau\, \epsilon^2(\tau)/2 = \int d\tau |E(\tau)|^2$ in the RWA]

$$J(t_f;\boldsymbol{\beta}) = A(t_f,\boldsymbol{\beta}) - \gamma\left(\int_{t_0}^{t_f} d\tau |E(\tau,\boldsymbol{\beta})|^2 - 1 \right)^2, \tag{52}$$

where γ is an adjustable positive constant. As γ becomes larger, the constraint is more rigidly satisfied. However, the exact value of γ is problem dependent. In general, we begin with a value of γ that is $\sim 1\%$ of the value of the yield for the initial guess of the parameters and then minimize the function in Eq. (52). Provided that this minimization is successful [in the sense that a finite value of $A(t_f;\boldsymbol{\beta})$ is found], the value of γ is multiplied by 10, the $\boldsymbol{\beta}$ values from the previous minimization are used as initial guesses in the minimization with the new value of γ, and new values of $\boldsymbol{\beta}$ are calculated. This procedure is repeated until the values of $\boldsymbol{\beta}$ do not change.

We perform the minimization using the standard conjugate gradient method.[31] Gradient methods require knowledge of the partial derivatives of the function with respect to the parameters. Fortunately, these derivatives are easy to obtain since the material function M_e^S is independent of the parameters. Thus, the partial derivatives of the functional $J(t_f,\boldsymbol{\beta})$ with respect to parameters $\boldsymbol{\beta}$ are given by

$$\frac{\partial J(t_f;\boldsymbol{\beta})}{\partial \boldsymbol{\beta}} = \frac{\partial A(t_f;\boldsymbol{\beta})}{\partial \boldsymbol{\beta}} - 2\gamma\, \mathrm{Re}\left(\int_{t_0}^{t_f} d\tau\, E^*(\tau;\boldsymbol{\beta}) \frac{\partial E(t;\boldsymbol{\beta})}{\partial \boldsymbol{\beta}} \right) \times \left(\int_{t_0}^{t_f} d\tau \left| E(t;\boldsymbol{\beta}) \right|^2 - 1 \right), \tag{53}$$

where

$$\frac{\partial A(t_f;\boldsymbol{\beta})}{\partial \boldsymbol{\beta}} = 2\,\mathrm{Re} \int_{t_0}^{t_f} d\tau \int_{t_0}^{t_f} d\tau'\, M_e^S(\tau,\tau') \times \frac{\partial E^*(\tau;\boldsymbol{\beta})}{\partial \boldsymbol{\beta}} E(\tau';\boldsymbol{\beta}). \tag{54}$$

Thus, given an M_e^S function and a functional form for $E(t;\boldsymbol{\beta})$, all the derivatives necessary to implement the conjugate gradient method can be calculated analytically.

We have performed the nonlinear optimization described here for the three systems discussed above. In all three cases, we have found that the parameter values change insignificantly from those found in the nonlinear least-squares fit. The results for these systems (for which there is only a single eigenvalue of M_e^S that differs significantly from zero) can be explained by a more detailed examination[34] of the weak field control equations than is appropriate here. However, for other systems in which there is more than one nonzero eigenvalue of the material function, nonlinear optimization can give a parametrized field with a significantly higher achievement than that of a field calculated from a nonlinear fit.[34]

V. SUMMARY, DISCUSSION, AND CONCLUSION

We have used realistic molecular potentials to demonstrate that simple and robust light fields with experimentally feasible parameters can be used to control wave-packet motion in diatomic molecules. The calculations presented herein are based on the density matrix formulation of molecular control theory developed by Yan *et al.*[9] This theory gives the globally optimal weak electric field as the eigenvector of a matrix that depends only on the desired target and the dynamics of the molecule in the absence of the external field, and thereby on the underlying molecular potential energy surfaces and transition dipole moments. In general, targets for control of quantum dynamics can always be specified in a phase space representation, and we have chosen to do that here.

We have demonstrated the application of this theory to three example systems: an I_2 molecular cannon, an I_2 molecular reflectron, and a multipulse Na_2 wave-packet focuser. In each case, we use quantum control to overcome the natural tendency for quantum wave packets to spread. The cannon focuses an outgoing wave packet in the I_2 B state continuum to form, at a specified time, a narrow

(minimum uncertainty) distribution centered about a chosen position and momentum. The unrestricted globally optimal field that produces this wave packet shows a substantial positive chirp, consistent with a classical physical picture in which the lower energy portions of the continuum wave packet on the B state are created first because they take longer to reach the target state than the higher energy components.

The reflectron focuses an incoming wave packet in the bound region of the I_2 B state, at a chosen time with a chosen minimum uncertainty distribution in both position and momentum. In this case, the globally optimal electric field has a substantial negative chirp, such that the higher energy portion of the wave packet is created before the lower energy portion. This result is consistent with a physical picture in which the high energy (but still bound) portions of the wave packet take longer to reach the target state due to their longer vibrational periods on the anharmonic potential energy curve.

In the strong field regime, the use of chirped pulses has proved useful, both theoretically[2,32,35–40] and experimentally,[41–44] in the control of population inversion in multilevel molecular and atomic systems or in a dephasing or inhomogeneous medium. The effect of the chirp is related to the adiabatic following of the material population dynamics by the field in order to achieve an effective π pulse for either sequential population inversions in multilevel systems[36,38,39] or for locking of the population inversion.[32,35,40–44] Recently, chirped pulses have also been used to study the dynamics of molecules in solution,[45–47] where it was shown that experiments using optical coherence with chirped pulses can yield unique information about the nature of the system-bath coupling. In the present work, we have demonstrated that chirped pulses can be used to focus a molecular wave packet about a given point in phase space at a specified target time. The use of a (nonoptimal) positively chirped field to create a localized dissociative molecular wave packet has also been proposed independently by Heller.[19] In our molecular cannon, the chirped pulse is a natural result of our optimal control eigenequation. We did not have to assume *a priori* that the control field is chirped.

In the case of Na_2 molecular wave-packet focusing, the minimum uncertainty target wave packet is created by a globally optimal superposition of three wave packets, each brought to the excited A state by a separate phase-locked pulse in the electric field. The pulses occur with time delays equal to the vibrational period of the molecule at the target energy, so that coherent addition of the amplitudes excited from the ground state can occur. All three pulses are chirped in such a way as to best cancel the dispersive effects of the anharmonicity of the potential which otherwise lead to spreading of the wave packet. It is also possible to create "squeezed states"[48–50] of matter in either position or momentum. We will discuss this point elsewhere.[34]

We have further demonstrated, for each case considered, that the globally optimal fields can be well fit by a parametrized electric field which should be experimentally realizable. The best-fit fields are shown to give achievements (as measured by how well the controlled wave packet overlaps the target wave packet) that are close to those of the unrestricted globally optimal fields. That it is not necessary to reproduce the exact forms of the globally optimal fields in order to obtain high achievements illustrates the robustness of these fields. We have also shown that it is in general possible to optimize the fitted parameters with respect to the achievement, which may lead to higher yields.

We believe that the simplicity and robustness of the globally optimal weak fields presented here, in contrast to the complexity and nonrobustness of many of the fields derived from iterative (and often strong field) quantum control calculations, may not be accidental. One reason may be the simple nature of the minimum uncertainty targets we have chosen here. Another reason may be that the fields we calculate are extremal eigenfunctions of a Hermitian matrix. As an analogy, one can consider the spectrum of the Schrödinger equation, in which the extremal (in this case minimum energy or ground state) eigenfunction is always the simplest, in the sense that it has the fewest nodes (e.g., the harmonic oscillator, particle in a box, or hydrogen atom ground states). It can be expected that iterative solutions of the control problem for complicated systems will tend to converge toward *locally* optimal solutions, which may lack the simplicity and robustness of the *globally* optimal electric fields. However, the strong field regime is of great interest because it allows dynamical behavior not possible with weak fields. We explore these issues in more detail elsewhere.[34]

The weak field theoretical approach discussed in this paper can be used to treat other aspects of quantum control as well. For strong field calculations, the globally optimal eigenfunction (or a superposition of the highest yield eigenfunctions) can be the starting point for iterative calculations. Solutions for quantum control involving multiple interactions with the light field can be constructed from globally optimal solutions of single field interactions.

We wish to conclude this paper with a brief discussion of how the focusing presented in this paper might in principle be observed experimentally. Observation of focused wave packets in the bound internuclear distance regions of excited state potentials is possible through ultrafast pump-probe spectroscopy, provided that an excited state is available with a reasonable Franck–Condon overlap in the internuclear region in which the wave packet is focused. Under these circumstances, pump-probe spectroscopy at the proper probe frequency will give a measure of the achievement, since it gives a signal which is related to the distribution of internuclear distances sampled by the time-dependent wave function. Similar considerations apply to pump-dump spectroscopy, in which the dump pulse returns the system to the ground electronic state. We note that many elements of these type of experiments are present in the ultrafast pump-probe experiments of several groups[51–54] on such systems as I_2, NaI, and Na_2, as well as in the I_2 pump-dump experiments with phase-locked pulses of Scherer, Fleming and co-workers,[4,33,55] and the recent

TABLE IV. Potential parameters for I_2 potential energy curves.

	X	B
T_e (cm^{-1})	0	15 769.0
r_e (Å)	2.666 3	3.024 8
D (cm^{-1})	12 440.1	4 381.29
a_0 (cm^{-1})	307 284.0	138 234.0
a_1	−3.842 87	−4.631 21
η	1.976 74	2.301 42
$10^{-5}c_5$ (cm^{-1} Å^5)	0.001 2	3.68
$10^{-6}c_6$ (cm^{-1} Å^6)	0.13	1.24
$10^{-8}c_8$ (cm^{-1} Å^8)	0.60	0.39
R_c (Å)	3.797 6	3.703 168
s_L (Å)	0.768 076	1.098 45

O_3 transient pump-dump experiments of Chen and coworkers.[56]

As we mentioned in the discussion of the molecular cannon, ultrafast electron and x-ray diffraction in principle can be used to probe focused atomic wave packets which are likely to be inaccessible to ultrafast spectroscopy. For the cannon, preliminary simulations show that ultrafast diffraction techniques might be able to image the focused state, even when that state has a large internuclear separation. Experiments are currently in preparation in our group to attempt to observe quantum control as described here via both ultrafast spectroscopy[27] and ultrafast diffraction.[26]

ACKNOWLEDGMENTS

We thank Richard Gillilan, Moshe Shapiro, and David Tannor for useful discussions, and Vladislav Yakovlev for the ultrafast diffraction simulations. The calculations in this paper were performed on the Cray Y-MP at the San Diego Supercomputer Center.

APPENDIX A: CONTROL OBJECTIVE IN TERMS OF THE SYMMETRIZED MOLECULAR FUNCTION

In this Appendix, we present a detailed derivation of Eq. (24). The derivation of Eq. (12) from Eq. (3) is similar. We begin by substituting Eqs. (19) and (23) into the integrand of Eq. (6). We have

$$\begin{aligned} &M(t_f-\tau_2,\tau_2-\tau_1)\epsilon(\tau_2)\epsilon(\tau_1) \\ &\quad=2\,\mathrm{Re}\{M_e(t_f-\tau_2,\tau_2-\tau_1)[E^*(\tau_2)E(\tau_1) \\ &\qquad+E(\tau_2)E^*(\tau_1)e^{-i2\omega_{eg}(\tau_2-\tau_1)} \\ &\qquad+E(\tau_2)E(\tau_1)e^{-i2\omega_{eg}\tau_2}+E^*(\tau_2)E^*(\tau_1)e^{i2\omega_{eg}\tau_1}]\}. \end{aligned} \tag{A1}$$

Only the first term in the above equation will survive after the temporal integration, since the other three terms contain ω_{eg}. These highly oscillatory factors will make a negligibly small contribution to the temporal integration compared to that from the first term. The neglect of these highly oscillatory terms is known as the RWA with respect to the electronic or optical transition. We have, therefore, in the RWA

$$\begin{aligned} A(t_f)&=2\hbar^{-2}\,\mathrm{Re}\int_{t_0}^{t_f}d\tau_2\int_{t_0}^{\tau_2}d\tau_1 M_e \\ &\quad\times(t_f-\tau_2,\tau_2-\tau_1)E^*(\tau_2)E(\tau_1). \end{aligned} \tag{A2}$$

By changing the order of the integration and exchanging the dummy integration variables, τ_2 and τ_1, Eq. (A2) can be recast as

$$\begin{aligned} A(t_f)&=2\hbar^{-2}\,\mathrm{Re}\int_{t_0}^{t_f}d\tau_2\int_{\tau_2}^{t_f}d\tau_1 M_e \\ &\quad\times(t_f-\tau_1,\tau_1-\tau_2)E^*(\tau_1)E(\tau_2) \\ &=2\hbar^{-2}\,\mathrm{Re}\int_{t_0}^{t_f}d\tau_2\int_{\tau_2}^{t_f}d\tau_1 M_e^* \\ &\quad\times(t_f-\tau_1,\tau_1-\tau_2)E(\tau_1)E^*(\tau_2). \end{aligned} \tag{A3}$$

Adding Eqs. (A2) and (A3), we obtain

$$\begin{aligned} 2A(t_f)&=2\,\mathrm{Re}\int_{t_0}^{t_f}d\tau_2\int_{t_0}^{t_f}d\tau_1 M_e^S(\tau_2,\tau_1) \\ &\quad\times E^*(\tau_2)E(\tau_1), \end{aligned} \tag{A4}$$

with

$$\begin{aligned} M_e^S(\tau_2,\tau_1)&=\hbar^{-2}M_e(t_f-\tau_2,\tau_2-\tau_1), \quad \tau_2>\tau_1 \\ M_e^S(\tau_2,\tau_1)&=\hbar^{-2}M_e^*(t_f-\tau_1,\tau_1-\tau_2), \quad \tau_2<\tau_1 \end{aligned} \tag{A5}$$

Equations (A5) are equivalent to Eq. (25). Since M_e^S is Hermitian, we can omit the Re sign in Eq. (A4) and thereby recover Eq. (24).

APPENDIX B: POTENTIAL ENERGY CURVES FOR I_2

We express the form of the potential for both the ground X and the excited B states as

$$\begin{aligned} V(r)&= \begin{cases} V_<(r), & r<R_c-s_L \\ f[(r-R_c)/s_L]V_<(r) & \\ \quad+\{1-f[(rR_c)/s_L]\}V_>(r), & R_c-s_L<r<R_c+s_L \\ V_>(r), & r>R_c+s_L. \end{cases} \end{aligned} \tag{B1}$$

Here, $V_<(r)$ is used for small diatomic distances:[57]

$$V_<(r)=a_0(1-r/r_e)^2[1-a_1(r_e/r)^\eta(1-r/r_e)], \tag{B2}$$

and $V_>(r)$ for large diatomic distances:[58]

$$V_>(r)=D_0-\left(\frac{c_5}{r^5}+\frac{c_6}{r^6}+\frac{c_8}{r^8}\right). \tag{B3}$$

These two functions are bridged smoothly (up to the second derivative) across the region $[R_c-s_L,R_c+s_L]$ via the smoothing function

$$f(s)=0.5-\frac{s}{16}(15-10s^2+3s^4). \tag{B4}$$

The constants r_e in Eq. (B2) and D_0 in Eq. (B3) are the potential minimum and the dissociation energy, respec-

tively. The other parameters in Eqs. (B2) and (B3) are obtained by a nonlinear fit to the available experimental Rydberg–Klein–Rees (RKR) points in Refs. 20 and 59. Together with the bridging position R_c and smoothing length s_L, these parameters are tabulated in Table IV for both the X and the B state potentials. This fit to the I_2 potential gives an accuracy of $<1\ \mathrm{cm}^{-1}$ for all of the available RKR points on both the X and B states.

[1] A. M. Weiner and J. P. Heritage, Rev. Phys. Appl. **22**, 1619 (1987).
[2] W. S. Warren and M. S. Silver, Adv. Magn. Reson. **12**, 247 (1988).
[3] J. T. Fourkas, W. L. Wilson, G. Wackerle, A. E. Frost, and M. D. Fayer, J. Opt. Soc. Am. B **6**, 1905 (1989).
[4] N. F. Scherer, A. J. Ruggiero, M. Du, and G. R. Fleming, J. Chem. Phys. **93**, 856 (1990).
[5] P. Brumer and M. Shapiro, Annu. Rev. Phys. Chem. **43**, 257 (1992).
[6] H. Rabitz and S. Shi, Adv. Mol. Vib. Coll. Dyn. **1A**, 187 (1991).
[7] S. A. Rice, Science **258**, 412 (1992).
[8] W. S. Warren, H. Rabitz, and M. Dahleh, Science **259**, 1581 (1993).
[9] Y. J. Yan, R. E. Gillilan, R. M. Whitnell, K. R. Wilson, and S. Mukamel, J. Phys. Chem. **97**, 2320 (1993).
[10] Y. J. Yan and S. Mukamel, J. Chem. Phys. **89**, 5160 (1988).
[11] U. Fano, Rev. Mod. Phys. **29**, 74 (1957).
[12] R. Kosloff, S. A. Rice, P. Gaspard, S. Tersigni, and D. J. Tannor, Chem. Phys. **139**, 201 (1989).
[13] J. Somloi and D. Tannor (unpublished).
[14] M. Shapiro and P. Brumer, Chem. Phys. Lett. **208**, 153 (1993).
[15] P. I. Richards, *Manual of Mathematical Physics* (Pergamon, New York, 1959).
[16] B. Kohler *et al.*, J. Phys. Chem. (in press).
[17] Y. J. Yan and S. Mukamel, J. Chem. Phys. **88**, 5735 (1988).
[18] E. J. Heller, Acc. Chem. Res. **14**, 368 (1981).
[19] E. J. Heller (private communication).
[20] R. F. Barrow and K. K. Yee, J. Chem. Soc. Faraday Trans. 2 **69**, 684 (1973).
[21] J. Paye, IEEE J. Quantum Electron. **QE-28**, 2262 (1992).
[22] J. C. Williamson and A. H. Zewail, Proc. Natl. Acad. Sci. USA **88**, 5021 (1991).
[23] J. C. Williamson, M. Dantus, S. B. Kim, and A. H. Zewail, Chem. Phys. Lett. **196**, 529 (1992).
[24] P. Bado *et al.*, Laser Chem. **3**, 231 (1983).
[25] J. P. Bergsma, M. H. Coladonato, P. M. Edelsten, J. D. Kahn, K. R. Wilson, and D. R. Fredkin, J. Chem. Phys. **84**, 6151 (1986).
[26] F. Raksi, C. Rose-Petruck, K. R. Wilson, and V. V. Yakovlev (unpublished).
[27] B. Kohler, F. Raksi, K. R. Wilson, and V. V. Yakovlev (unpublished).
[28] J. N. Bardsley, B. R. Junker, and D. W. Norcross, Chem. Phys. Lett. **37**, 502 (1976).
[29] B. Amstrup, R. J. Carlson, A. Matro, and S. A. Rice, J. Phys. Chem. **95**, 8019 (1991).
[30] G. R. Fleming, *Chemical Applications of Ultrafast Spectroscopy* (Oxford, London, 1986).
[31] W. H. Press, B. P. Flannery, S. A. Teukolsky, and W. T. Vetterling, *Numerical Recipes: The Art of Scientific Computing* (Cambridge University, Cambridge, 1986).
[32] L. Allen and J. H. Eberly, *Optical Resonance and Two-Level Atoms* (Dover, New York, 1987).
[33] N. F. Scherer, R. J. Carlson, A. Matro, M. Du, A. J. Ruggiero, V. Romero-Rochin, J. A. Cina, G. R. Fleming, and S. A. Rice, J. Chem. Phys. **95**, 1487 (1991).
[34] J. L. Krause, R. M. Whitnell, K. R. Wilson, and Y. J. Yan (unpublished).
[35] E. B. Tready, Phys. Lett. A **27**, 421 (1968).
[36] S. Chelkowski, A. Bandrauk, and P. B. Corkum, Phys. Rev. Lett. **65**, 2355 (1990).
[37] S. Ruhman and R. Kosloff, J. Opt. Soc. Am. B **7**, 1748 (1990).
[38] S. Chelkowski and A. D. Bandrauk, Phys. Rev. Lett. **186**, 264 (1991).
[39] B. Just, J. Manz, and I. Trisca, Chem. Phys. Lett. **193**, 423 (1992).
[40] D. Goswami and W. S. Warren, J. Chem. Phys. (1993).
[41] E. B. Tready and A. J. Demaria, Phys. Lett. A **29**, 369 (1969).
[42] D. Grischkowsky, Phys. Rev. A **7**, 2096 (1973).
[43] C. Liedenbaum, S. Stolte, and J. Reuss, Phys. Rep. **178**, 1 (1989).
[44] J. S. Melinger, A. Hariharan, S. R. Gandhi, and W. S. Warren, J. Chem. Phys. **95**, 2210 (1991).
[45] T. Tokizaki, Y. Ishida, and T. Yajima, Opt. Commun. **71**, 355 (1989).
[46] E. T. J. Nibbering, D. A. Wiersma, and K. Duppen, Phys. Rev. Lett. **68**, 514 (1992).
[47] K. Duppen, F. de Haan, E. T. J. Nibbering, and D. A. Wiersma, Phys. Rev. A **47**, 5120 (1993).
[48] A. V. Vinogradov and J. Janszky, in *Ultrafast Phenomena VIII* (Springer, Berlin, 1992).
[49] T. J. Dunn, J. N. Sweetser, I. A. Walmsley, and C. Radzewicz, Phys. Rev. Lett. **70**, 3388 (1993).
[50] I. Averbukh and M. Shapiro, Phys. Rev. A **47**, 5086 (1993).
[51] L. R. Khundkar and A. H. Zewail, Annu. Rev. Phys. Chem. **41**, 15 (1990).
[52] A. H. Zewail, Faraday Discuss. Chem. Soc. **91**, 207 (1991).
[53] T. Baumert, V. Engel, C. Röttgermann, W. T. Strunz, and G. Gerber, Chem. Phys. Lett. **191**, 639 (1992).
[54] T. Baumert, V. Engel, C. Meier, and G. Gerber, Chem. Phys. Lett. **200**, 488 (1992).
[55] N. F. Scherer, A. Matro, L. D. Ziegler, M. Du, R. J. Carlson, J. A. Cina, and G. R. Fleming, J. Chem. Phys. **96**, 4180 (1992).
[56] Y. Chen, L. Hunziker, P. Ludowise, and M. Morgon, J. Chem. Phys. **97**, 2149 (1992).
[57] M. K. Matzen, G. V. Calder, and D. K. Hoffman, Spectrochim. Acta **29A**, 2005 (1973).
[58] R. J. LeRoy, J. Chem. Phys. **52**, 2678 (1970).
[59] J. A. Coxon, J. Quant. Spectrosc. Radiat. Transfer **11**, 443 (1971).